# Electron Transport in Graphene Nanoribbon Field-Effect Transistor under Bias and Gate Voltages: Isochemical Potential Approach

Jeonghun Yun,[†,‡] Geunsik Lee,*,[†] and Kwang S. Kim*,[†]

[†]Department of Chemistry, Ulsan National Institute of Science and Technology (UNIST), Ulsan 44919, Korea
[‡]Department of Chemistry, Pohang University of Science and Technology, Pohang 37673, Korea

S *Supporting Information*

ABSTRACT: Zigzag graphene nanoribbon (zGNR) of narrow width has a moderate energy gap in its antiferromagnetic ground state. So far, first-principles electron transport calculations have been performed using nonequilibrium Green function (NEGF) method combined with density functional theory (DFT). However, the commonly practiced bottom-gate control has not been studied computationally due to the need to simulate an electron reservoir that fixes the chemical potential of electrons in the zGNR and electrodes. Here, we present the isochemical potential scheme to describe the top/back-gate effect using external potential. Then, we examine the change in electronic state under the modulation of chemical potential and the subsequent electron transport phenomena in zGNR transistor under substantial top-/back-gate and bias voltages. The gate potential can activate the device states resulting in a boosted current. This gate-controlled current-boosting could be utilized for designing novel zGNR field effect transistors (FETs).
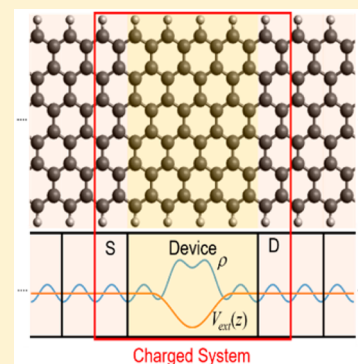
Owing to its ballistic transport property, graphene[1,2] exhibits high electron mobility. It could resolve the scale-down issue in nanoscale transistors. However, the absence of band gap in pristine graphene precludes its use in FET without modification.[3] Graphene nanoribbon (GNR), one of the graphene derivatives with a small band gap, has been intensively studied as a viable material for graphene-based devices.[4−13] Various efforts to open a bandgap in graphene have been made, such as top-down/bottom-up synthesis of GNR with finite width,[14,15] dual doping of bilayer graphene,[16,17] and functionalization of graphene.[18] To realize GNR as a transistor, it is essential to investigate such feasibility based on theoretical understanding that could attract experimental demonstrations. Model calculations predict that the band gap of zGNR is closed upon charging,[19,20] whereas the nonequilibrium transport study for open systems was not reported, to the best of our knowledge. Instead of modifying the occupation number with fixed single-particle orbitals, we need to self-consistently consider the chemical potential equilibrium of electrons between the device and electrodes. Because the electron is free to move to and from the back-gate, applying a back-gate voltage modifies chemical potential of the device-gate system. However, its effect on transmission has hardly been studied in first-principles calculations. Top-gate voltage, considered as a local perturbation potential, can be studied by adding an external potential to a device part.[21,22] However, a further consideration of the charged device part in the presence of a moderate gate potential (V_g) of ∼1 eV has yet to be made.

On the basis of the commonly used DFT-NEGF method,[7,23,24] for the first time, we implement the isochemical potential (iso-μ) scheme to study electron transport of GNR under varying V_g which substantially modifies μ. Of course,

modification of the electrostatic potential in the device arising from bias voltage (V_b) is taken into account using the Poisson equation. We minimize the total energy ($E - \mu N_e$) by controlling the total number of electrons (N_e) under Fermi−Dirac distribution in the system to obtain a given μ at temperature T. This Fermi−Dirac distribution implicitly takes into account the TS term (S: entropy), and so the system energy corresponds to E-TS-μN_e, which is associated with grand canonical ensemble approach. For this calculation, we choose a zGNR with a width of six carbon atoms (6-zGNR) as an example, where the electronic structure varies with respect to μ and N_e. First-principles band calculations of the unit 6-zGNR system having the initial antiferromagnetic (AFM) ordering in the charge-neutral state are performed at varying Fermi levels. The relative stability of AFM and FM phases is compared for the systems with same charging level $\Delta \underline{n}$. After showing the homogeneous charging effect on the electron transport, we also show a local charging effect that emulates the top gate.

Spin-resolved transmission functions of 6-zGNR are calculated using POSTRANS.[24,25] Geometry of edge-hydrogenated 6-zGNR is optimized using the Perdew−Burke−Ernzerhof (PBE) functional,[26] single-ζ polarization basis set, Troullier−Martins pseudopotential,[27] and cutoff energy of 300 Ry. Temperature 300 K is used for the Fermi−Dirac distribution throughout this work.

On the basis of Landauer−Büttiker formalism, the source-drain current (I) at V_b is

$$I(V_b) = \frac{2e}{h} \int T(E, V_b, N_e)[f(E - \mu_L) - f(E - \mu_R)]dE \tag{1}$$

We assume that $\mu_{L/R} = \pm V_b/2$ for the left/right (L/R) electrode. The Fermi−Dirac function $f(E - \mu_{L/R})$ at energy E depends on V_b. The transmission probability is expressed as the trace of transmission matrix

$$T(E, V_b, N_e) = Tr[\Gamma_L G \Gamma_R G^\dagger] \tag{2}$$

where $\Gamma_{L/R} = i[\Sigma_{L/R} - \Sigma_{L/R}^\dagger]$, $\Sigma_{L/R}$ is self-energy, and Green's function is

$$G = [E - H_C - \Sigma_L(E) - \Sigma_R(E)]^{-1} \tag{3}$$

Here, H_c is the device Hamilitonian.

The transmission matrix is diagonalized in orbital basis using Inelastica package[28] to yield the eigenchannels and corresponding transmission values.

Because the orbital-based DFT method calculates individual orbital occupancies by filling the orbitals according to $f(E - \mu_{L/R})$, the N_e does not need to be an integer. Instead of determining μ for the given N_e (as normal DFT calculations do), we choose a constant μ and determine the corresponding N_e

$$N_e = \int_{-\infty}^{\infty} D(E) f(E - \mu) dE \tag{4}$$

where $D(E)$ is the density of states at E. DFT eigenstates are highly dependent on N_e, so it must be gradually modified in order to avoid divergence. N_e is varied until the corresponding μ is within 0.5 meV of the desired value.

The charged systems require compensating charges to prevent the divergence of electrostatic energy. In usual cases, the fast-Fourier-transform (FFT)-based Poisson solver resolves the problem by ignoring $\mathbf{G} = 0$ in the Poisson equation $V(\mathbf{G}) = -4\pi\rho(\mathbf{G})/\mathbf{G}^2$ ($\mathbf{G}$: reciprocal lattice vector), equivalent to adding the homogeneous compensating charge inside the cell. However, description of low-dimensional charged systems using atom-centered basis set is restricted by the inability of the basis set to cover the compensating charge in the vacuum space. Therefore, all the compensating charges are added on the atom center to avoid unphysical error in Hartree energy. The compensating charges affect only the electrostatic potential because it is removed before exchange-correlation energy calculation.

Introducing fractional charge can be justified in the sense of electronic doping, where the metallic substrate either donates or withdraws electron, without affecting electronic structure of the device. However, error in electrostatic energy is inevitable to some extent due to the interaction of compensating charge and the electron density of the system. For this reason, the total energy is not precisely $E - \mu N$. Thus, comparison of two electronic states is possible only if the states of interest have the same compensating charge.

Figure 1 and Table 1 illustrate the calculation results. Charge-neutral AFM 6-zGNR has a band gap of 0.61 eV, with double dispersions at valence and conduction bands. The depth of second dispersion is 0.24 eV for the valence band and 0.08 eV for the conduction band. For small charge modification, as charge per unit cell $|\Delta n|$ changes from 0 to ~0.1, the relative stabilization of the AFM state over the FM state decreases. The transition from the AFM to FM state arises at $\Delta n < -0.047$ e/cell or $\Delta n > 0.057$ e/cell. The AFM state of zGNR is quite
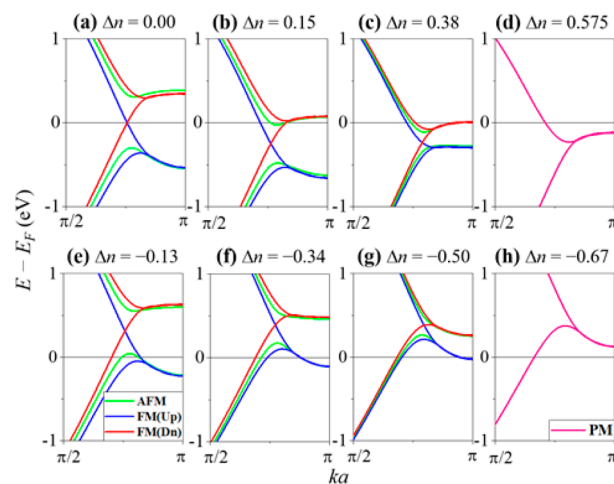

Figure 1. Band structures of 6-zGNR at varying total charge of the device (or varying μ). (a) Pristine zGNR band structure at the noncharged state. Black/blue/red lines correspond to AFM/FM(spin up)/FM(spin down). (b−d) Cases for up-shifted Fermi levels. The FM state is more stable, while the AFM gap still retains (b). A Fermi level shift causes flat FM spin-up states (c). At high Fermi energy levels outside the AFM double dispersion region, the system becomes PM (d). (e−h) Cases for down-shifted Fermi levels. A flat FM spin-down band occurs between (e) and (f). The second dispersion of the AFM conduction band also vanishes (f). At low Fermi energy levels, the PM state is the most stable (g).

Table 1. Chemical potential changes[a], AFM-FM energy differences, and most stable spin states[b] at varying charge per unit cell[c] of 6-zGNR.[d]

Δn	$\Delta\mu_{AFM}$	$\Delta\mu_{FM}$	$E_{AFM} - E_{FM}$	spin state
−0.614	−0.65	−0.665		P
−0.509	−0.6	−0.616	1.1	F
−0.130	−0.35	−0.359	6.3	F
−0.0563	−0.3	−0.176	2.0	F
−0.0133	−0.25	−0.042	−8.3	AF
0.0	0.0	0.0	−12.9	AF
0.0164	0.25	0.051	−7.9	AF
0.150	0.3	0.287	3.6	F
0.380	0.35	0.345	0.5	F
0.500	0.4	0.391		P

[a]$\Delta\mu_{AFM}$, $\Delta\mu_{FM}$. [b]AF/F/P. [c]Δn. [d]$\Delta\mu$ are in eV; E in meV. AF, antiferromagnetic; F, ferromagnetic; P, paramagnetic.

stable under Fermi level modulation within the zGNR band gap. The ground state is AFM until $\Delta\mu_{AFM}$ is lower/higher than the first conduction/valence band edge, whereas it becomes FM when $\Delta\mu_{AFM} < -0.294$ eV or $\Delta\mu_{AFM} > 0.280$ eV (see Figure S1 for the relative stability of the AFM state over the FM state with respect to Δn.).

In the band diagram of Figure 1b,c,e−g, the AFM state retains the band gap in the stable FM region with a reduced band gap (<0.5 eV), whereas the system changes to FM if $\Delta\mu_{AFM}$ is greater than the AFM gap. Moreover, as in Figure 1c,f, we find the collapse of double dispersion of the AFM conduction/valence band, implying that the second dispersion is highly susceptible to μ-modulation. Changes in dispersion behavior of the FM spin-up valence and spin-down conduction bands are also found.

At an extreme charge modification listed in Table 1 and Figure 1d,h, the system converges to the paramagnetic (PM)

state regardless of initial spin configuration. Hence, as μ deviates from zero, the stable configuration changes from the AFM semiconductor to the FM metal, then to the PM metal, in agreement with the Hubbard model result.[20]

As μ changes, the electronic state undergoes phase transition. Thus, choosing the right phase (AFM/FM/PM) for the electrodes is important when calculating the zGNR system at a given μ. Because the given μ determines the electronic state of the specific phase, the electrode state and its coupling to the device should be recalculated for the updated μ. The back-gate voltage modifies μ over the whole device.

Here, we calculate the transmission probability at each charging level in Table 1. There is no transmission gap for the FM and PM metal cases. It is important to self-consistently take into account orbital relaxation caused by change in μ. Figure 2b−d shows an additional modification in the curve shape
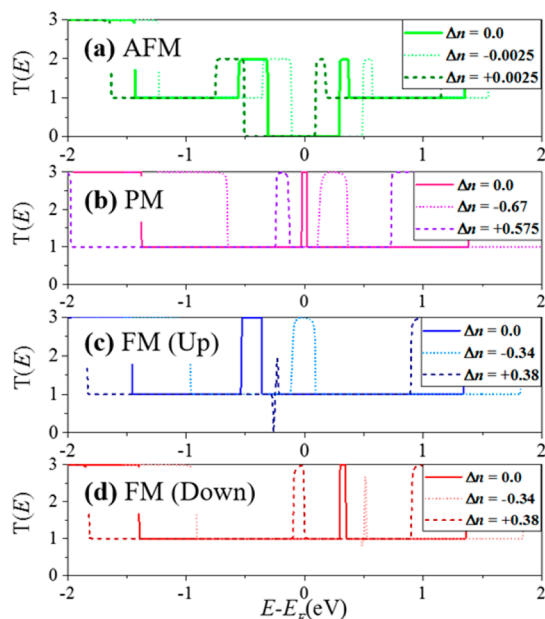

Figure 2. Transmission shifts in the 6-zGNR calculations at V_b = 0 V. Black lines as the reference represent the noncharged transmission at each magnetic state. The system consists of 12 cells; Δn is given per cell. (a) AFM region. $\Delta n = \pm 0.0025$ corresponds to $\Delta\mu_{AFM} = \pm 0.20$ eV. (b) PM region. $\Delta n = -0.67/+0.575$ corresponds to $\Delta\mu_{PM} = -0.684/+0.565$ eV. (c/d) FM spin-up/down region. $\Delta n = -0.34/+0.38$ corresponds to $\Delta\mu_{FM} = -0.527 + 0.326$ eV.

besides a simple shift toward positive or negative direction. Although the transmission in metal is not changed under charging, additional transmissions arising from multiple dispersion at a given Fermi level show substantial modulations, as expected from the modified band structure in Figure 1. For example, Figure 2c shows enhanced/suppressed transmission of spin-up electron in the positively/negatively charged condition. The transmission value of ~3.0 occurs at a band-overlapped region of FM states, and its width corresponds to the width of overlapped dispersion. The eccentric transmission near $E − E_F$ = −0.28 eV of a negatively charged case arises from the flat band formation of FM dispersion near $ka = \pi$, as in Figure 1c.

These results raise an important point on the conventional transport calculations. The commonly accepted pictures on nanodevice systems, where back-gate voltage operation is regarded as mere shift of μ with fixed band and transmission structures, should not be used when the electronic states are

susceptible to change upon charging. Consequently, the practically meaningful part of a transmission diagram at a given bias is strictly restricted within the bias window, because every transmission should be recalculated at different values of μ and V_b.

To simulate local potentials which are represented as nanoscale top-gate effects, we examine the transport in 6-zGNR at varying V_g on the central device segment, using the iso-μ scheme in grand canonical ensemble approach (Figure 3b). The application of V_g is mimicking the top-gate voltage. If
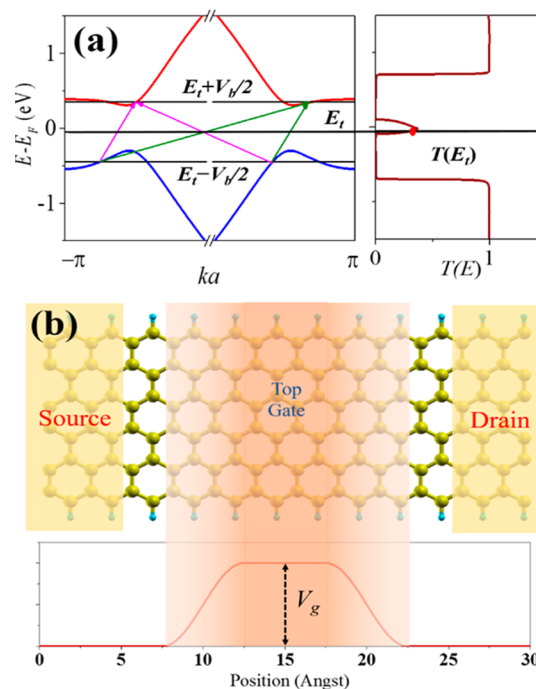

Figure 3. (a) Relation between source/drain band and transmission profiles. Green/magenta arrows stand for individual eigenchannels shown in the transmission curve. (b) Illustration of the calculated system with top-gate where the shape of external potential is schematically drawn.

the potential is lowered in a small region, then the electron is accumulated in that region of zGNR. Because the circuit is of macroscopic size, semi-infinite leads are regarded as an electron reservoir with fixed μ, so that the Fermi level will not be changed by small manipulation on the device part. DFT−NEGF calculations are performed on the system comprised of device and 1−2 units of source/drain electrode(s) representing infinite continuum. We choose $\Delta\mu = 0$ and then keep the electrode state as AFM throughout the calculation.

To adopt V_g as an independent variable while keeping μ fixed, we consider gate-controlled coupling of device and leads. The gate potential elevates the device energy level, but under the iso-μ, the number of device electrons is adjusted, resulting in the shifting of the valence/conduction band toward the Fermi level. We consider V_b as another independent variable because the gap between source and drain should be overcome by V_b.

The system consists of 12 blocks of 6-zGNR, the left/right 2 blocks were assigned as leads (source/drain), and the top-gated region was set as 6 blocks total, with 4 blocks of cutoff region. Square potential of depth V_g was added to the top-gated region, illustrated as shaded in Figure 3b. A cutoff function of the shape

$V_g(1 + \cos(\pi z/z_{cut}))/2$ was introduced to scale down the potential outside the given area.

The calculated transmission details for each V_b within the bias-induced conduction range are given in Figure S1. We note that the region with modified gate potential converges to the AFM configuration after reaching the self-consistency because the AFM-AFM coupling rather than others is favored for the gate length considered here. Thus, only one spin component has been plotted.

Transmission is modified according to V_g. Figure 4a is the representative result of transmission at $V_b = 0.8$ V. Two major
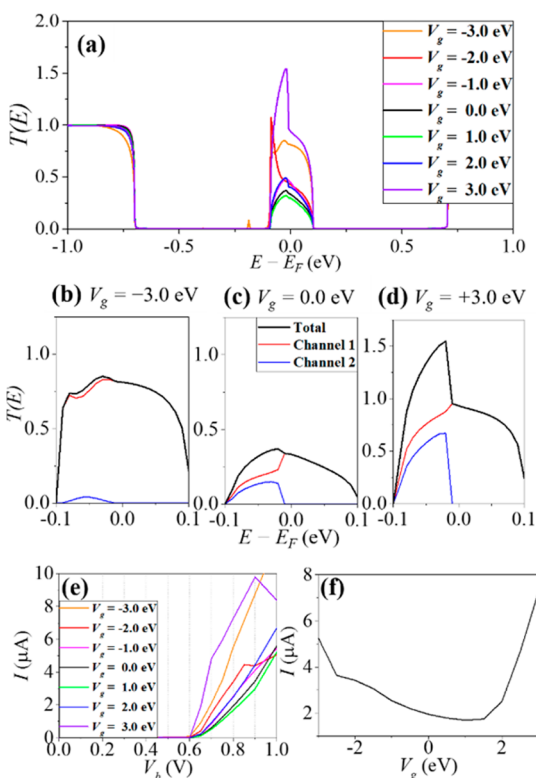

Figure 4. (a) Gate-control driven modulation of the transmission curve at $V_b = 0.8$ V. Transmission boosts at high V_b, but it is not symmetric. (b−d) Eigenchannel eigenvalues of transmission channel at varying V_g obtained from eigenchannel decomposition. The width of the two-channel region is 0.08 eV. Note that eigenchannels are ordered in terms of their magnitude. (e) $I–V_b$ curve of 6-zGNR at varying gate potentials V_g (threshold V_b: 0.6 V). (f) $I–V_g$ curve at $V_b = 0.8$ V. Current increases with increasing V_g.

transmission eigenchannels[28,29] exist in the region 0.6 V < V_b < 0.9 V, implying the existence of two terminals in conduction band, as in Figure 3a. This V_b window is the bias control range. The change made in V_g affects only the coupling parameter between source and drain states because the starting/terminal state is determined according to source/drain valence/conduction band. The transmission is found to be modulated controllably at large $|V_g|$, and just one of the two eigenchannels is active to the modulation by V_g. Figure 4b−d shows the eigenchannel analysis at extreme V_g's ($V_g = \pm 3.0$ eV). There is a smaller eigenchannel of width 0.08 eV within 0.7 V $\leq V_b < 0.9$ V. Thus, we deduce that the smaller eigenchannel originates from the transmission from the valence band to the smaller dispersion of conduction band. Consequently, the wider transmission originates from the large dispersion of 6-zGNR

conduction band. At $V_g = 3.0$ eV, the overall transmission is highly boosted and both eigenchannels are found to be activated, but at $V_g = -3.0$ eV only the eigenchannel originated from the larger dispersion is active.

The increase of transmission at extreme V_g could be compared with a simple tight-binding Hamiltonian, where the density of states of the device part shows parallel shift by V_g. If the number of active device states increases, the transmission and current will increase. The iso-μ condition regulates the electron occupancy of the device part, determining the number of states within the bias window. However, the transmission in orbitals is mainly governed by coupling between lead and device states, which should be recalculated for every new device states.

The $I−V$ characteristics of the system derived from the transmission data (Figure S1) are in Figure 4e,f. Figure 4e shows the $I−V$ curve for every gate potential (not gate voltage). Inside the bias control range, the $I−V_g$ curve shows the trend of Figure 4f, indicating that the gate-controlled current is well-described in first-principles calculations. Otherwise, outside the bias control range, the current does not follow the same trend, due to the partial collapse of AFM transmission.[30]

Expanding our study of zGNR to arbitrary semiconducting nanodevices, one can expect more than unit transmission (and more current) if more than one dispersion exists in a specific energy of conduction band. This can be either multiple dispersions within a band or multiple conduction bands at a specific point such as $3n + 1$ width armchair GNR. One may derive a new property if the band structure of the target system is sensitive to charging, such as spin-polarized current as expected in Figure 2.

In summary, we discussed an FET-like current modulation of 6-zGNR using DFT-NEGF formalism based on the gate-controlled iso-μ scheme in the presence of moderate V_b and V_g at 300 K. The transmission profiles of the charged zGNR were reported for the first time. They are highly dependent on band structures within charging effect, along with the magnetism. We were able to describe modulation of the electronic structure of the 6-zGNR system with respect to additional charging, along with the range of μ to keep the initial magnetism. Careful choice of gate potential can activate the initially inactive states and thus boost the current. This phenomenon could invoke experimental demonstrations for effective GNR-FET using bottom-up synthesized GNRs.

■ ASSOCIATED CONTENT

ⓢ Supporting Information

The Supporting Information is available free of charge on the ACS Publications website at DOI: 10.1021/acs.jpclett.6b00996.

> Figure S1 and S2. Figure S1 is for the relative stability of the AFM state over the FM state with respect to charging. Figure S2 is for the transmission curves on various V_b and V_g. (PDF)

■ AUTHOR INFORMATION

Corresponding Authors
*E-mail: kimks@unist.ac.kr.
*E-mail: gslee@unist.ac.kr.

Notes
The authors declare no competing financial interest.

■ REFERENCES

(1) Novoselov, K. S.; Geim, A. K.; Morozov, S. V.; Jiang, D.; Zhang, Y.; Dubonos, S. V.; Grigorieva, I. V.; Firsov, A. A. Electric Field Effect in Atomically Thin Carbon Films. *Science* **2004**, *306*, 666−669.

(2) Kim, K. S.; Zhao, Y.; Jang, H.; Lee, S. Y.; Kim, J. M.; Kim, K. S.; Ahn, J.-H.; Kim, P.; Choi, J.-Y.; Hong, B. H. Large-Scale Pattern Growth of Graphene Films for Stretchable Transparent Electrodes. *Nature* **2009**, *457*, 706−710.

(3) Meric, I.; Han, M. Y.; Young, A. F.; Ozyilmaz, B.; Kim, P.; Shepard, K. L. Current Saturation in Zero-Bandgap, Top-Gated Graphene Field-Effect Transistors. *Nat. Nanotechnol.* **2008**, *3*, 654−659.

(4) Yang, L.; Park, C. H.; Son, Y. W.; Cohen, M. L.; Louie, S. G. Quasiparticle Energies and Band Gaps in Graphene Nanoribbons. *Phys. Rev. Lett.* **2007**, *99*, 186801.

(5) Han, M. Y.; Ozyilmaz, B.; Zhang, Y.; Kim, P. Energy Band-Gap Engineering of Graphene Nanoribbons. *Phys. Rev. Lett.* **2007**, *98*, 206805.

(6) Son, Y.-W.; Cohen, M. L.; Louie, S. G. Half-Metallic Graphene Nanoribbons. *Nature* **2006**, *444*, 347−349.

(7) Kim, W. Y.; Kim, K. S. Prediction of Very Large Values of Magnetoresistance in a Graphene Nanoribbon Device. *Nat. Nanotechnol.* **2008**, *3*, 408−412.

(8) Muñoz-Rojas, F.; Fernández-Rossier, J.; Palacios, J. J. Giant Magnetoresistance in Ultrasmall Graphene Based Devices. *Phys. Rev. Lett.* **2009**, *102*, 136810.

(9) Saha, K. K.; Drndić, M.; Nikolić, B. K. DNA Base-Specific Modulation of μA Transverse Edge Currents Through a Metallic Graphene Nanoribbon with a Nanopore. *Nano Lett.* **2012**, *12*, 50−55.

(10) Kim, S.-W.; Kim, H.-J.; Choi, J.-H.; Scheicher, R. H.; Cho, J.-H. Contrasting Interedge Superexchange Interactions of Graphene Nanoribbons Embedded in h-BN and Graphane. *Phys. Rev. B: Condens. Matter Mater. Phys.* **2015**, *92*, 035443.

(11) Min, S. K.; Kim, W. Y.; Cho, Y.; Kim, K. S. Fast DNA Sequencing with a Graphene-Based Nanochannel Device. *Nat. Nanotechnol.* **2011**, *6*, 162−165.

(12) Nelson, T.; Zhang, B.; Prezhdo, O. V. Detection of Nucleic Acids with Graphene Nanopores: Ab Initio Characterization of a Novel Sequencing Device. *Nano Lett.* **2010**, *10*, 3237−3242.

(13) Feliciano, G. T.; Sanz-Navarro, C.; Coutinho-Neto, M. D.; Ordejón, P.; Scheicher, R. H.; Rocha, A. R. Capacitive DNA Detection Driven by Electronic Charge Fluctuations in a Graphene Nanopore. *Phys. Rev. Appl.* **2015**, *3*, 034003.

(14) Cai, J.; Ruffieux, P.; Jaafar, R.; Bieri, M.; Braun, T.; Blankenburg, S.; Muoth, M.; Seitsonen, A. P.; Saleh, M.; Feng, X.; et al. Atomically Precise Bottom-up Fabrication of Graphene Nanoribbons. *Nature* **2010**, *466*, 470−473.

(15) Magda, G. Z.; Jin, X.; Hagymási, I.; Vancsó, P.; Osváth, Z.; Nemes-Incze, P.; Hwang, C.; Biró, L. P.; Tapasztó, L. Room-Temperature Magnetic Order on Zigzag Edges of Narrow Graphene Nanoribbons. *Nature* **2014**, *514*, 608−611.

(16) Yang, J. W.; Lee, G.; Kim, J. S.; Kim, K. S. Gap Opening of Graphene by Dual FeCl3-Acceptor and K-Donor Doping. *J. Phys. Chem. Lett.* **2011**, *2*, 2577−2581.

(17) Park, J.; Jo, S. B.; Yu, Y. J.; Kim, Y.; Yang, J. W.; Lee, W. H.; Kim, H. H.; Hong, B. H.; Kim, P.; Cho, K.; et al. Single-Gate Bandgap Opening of Bilayer Graphene by Dual Molecular Doping. *Adv. Mater.* **2012**, *24*, 407−411.

(18) Georgakilas, V.; Otyepka, M.; Bourlinos, A. B.; Chandra, V.; Kim, N.; Kemp, K. C.; Hobza, P.; Zboril, R.; Kim, K. S. Functionalization of Graphene: Covalent and Non-Covalent Approaches, Derivatives and Applications. *Chem. Rev.* **2012**, *112*, 6156−6214.

(19) Lee, G.; Cho, K. Electronic Structures of Zigzag Graphene Nanoribbons with Edge Hydrogenation and Oxidation. *Phys. Rev. B: Condens. Matter Mater. Phys.* **2009**, *79*, 165440.

(20) Jung, J.; MacDonald, A. H. Carrier Density and Magnetism in Graphene Zigzag Nanoribbons. *Phys. Rev. B: Condens. Matter Mater. Phys.* **2009**, *79*, 235433.

(21) Yan, Q.; Huang, B.; Yu, J.; Zheng, F.; Zang, J.; Wu, J.; Gu, B.-L.; Liu, F.; Duan, W. Intrinsic Current-Voltage Characteristics of Graphene Nanoribbon Transistors and Effect of Edge Doping. *Nano Lett.* **2007**, *7*, 1469−1473.

(22) Saraiva-Souza, A.; Smeu, M.; Zhang, L.; Filho, A. G. S.; Guo, H.; Ratner, M. a. Molecular Spintronics: Destructive Quantum Interference Controlled by a Gate. *J. Am. Chem. Soc.* **2014**, *136*, 15065−15071.

(23) Stokbro, K.; Taylor, J.; Brandbyge, M.; Ordejón, P. TranSIESTA: A Spice for Molecular Electronics. *Ann. N. Y. Acad. Sci.* **2003**, *1006*, 212−226.

(24) Kim, W. Y.; Kim, K. S. Tuning Molecular Orbitals in Molecular Electronics and Spintronics. *Acc. Chem. Res.* **2010**, *43*, 111−120.

(25) Kim, W. Y.; Kim, K. S. Carbon Nanotube, Graphene, Nanowire, and Molecule-Based Electron and Spin Transport Phenomena Using the Nonequilibrium Green's Function Method at the Level of First Principles Theory. *J. Comput. Chem.* **2008**, *29*, 1073−1083.

(26) Perdew, J. P.; Burke, K.; Ernzerhof, M. Generalized Gradient Approximation Made Simple. *Phys. Rev. Lett.* **1996**, *77*, 3865−3868.

(27) Troullier, N.; Martins, J. L. Efficient Pseudopotentials for Plane-Wave Calculations. *Phys. Rev. B: Condens. Matter Mater. Phys.* **1991**, *43*, 1993−2006.

(28) Paulsson, M.; Brandbyge, M. Transmission Eigenchannels from Nonequilibrium Green's Functions. *Phys. Rev. B: Condens. Matter Mater. Phys.* **2007**, *76*, 115117.

(29) Jacob, D.; Palacios, J. J. Orbital Eigenchannel Analysis for Ab-Initio Quantum Transport Calculations. *Phys. Rev. B: Condens. Matter Mater. Phys.* **2006**, *73*, 075429.

(30) Areshkin, D. A.; Nikolić, B. K. I−V Curve Signatures of Nonequilibrium-Driven Band Gap Collapse in Magnetically Ordered Zigzag Graphene Nanoribbon Two-Terminal Devices. *Phys. Rev. B: Condens. Matter Mater. Phys.* **2009**, *79*, 205430.